

Geophysical Research Letters

RESEARCH LETTER

10.1029/2021GL093302

Key Points:

- The increase in cloud feedback in CESM can be mostly attributed to the ocean heat uptake evolution in the Southern Ocean
- The increasingly weakening of ocean heat uptake in the Southern Ocean leads to increasingly enhanced warming locally and remotely
- The remote impact on the tropical surface temperature pattern leads to an increase in cloud feedback by decreasing tropospheric stability

Supporting Information:

Supporting Information may be found in the online version of this article.

Correspondence to:

Y.-T. Hwang,
ythwang@ntu.edu.tw

Citation:

Lin, Y.-J., Hwang, Y.-T., Lu, J., Liu, F., & Rose, B. E. J. (2021). The dominant contribution of Southern Ocean heat uptake to time-evolving radiative feedback in CESM. *Geophysical Research Letters*, 48, e2021GL093302. <https://doi.org/10.1029/2021GL093302>

Received 20 AUG 2020

Accepted 14 APR 2021

The Dominant Contribution of Southern Ocean Heat Uptake to Time-Evolving Radiative Feedback in CESM

Yuan-Jen Lin¹ , Yen-Ting Hwang¹ , Jian Lu² , Fukai Liu³ , and Brian E. J. Rose⁴ 

¹Department of Atmospheric Sciences, National Taiwan University, Taipei, Taiwan, ²Atmospheric Sciences and Global Change Division, Pacific Northwest National Laboratory, Richland, WA, USA, ³Key Laboratory of Physical Oceanography, Institute for Advanced Ocean Studies, Ocean University of China and Qingdao National Laboratory for Marine Science and Technology, Qingdao, China, ⁴Department of Atmospheric and Environmental Sciences, University at Albany, State University of New York, Albany, NY, USA

Abstract In most fully coupled climate models, the net radiative feedback magnitude decreases with time after abruptly quadrupling CO₂. Hypotheses have been raised to explain the time dependence of radiative feedbacks, including the influence from surface warming pattern and ocean heat uptake (OHU) pattern. By using the Green's Function derived from pairs of simulations in the atmospheric model (CAM5) coupled with a slab-ocean, with each simulation being forced by a localized surface heat flux anomaly, we evaluate the influences of regional OHU on transient surface warming pattern, accounting for the changes in radiative feedbacks. The attribution of the time-evolving net radiative feedback highlights the remote impact from OHU over the Southern Ocean on tropical sea surface temperature. The time-dependent weakening of OHU over the Southern Ocean gives rise to increasingly enhanced surface warming in southeastern Pacific, which leads to decreasing tropospheric stability and more positive cloud feedback decades after quadrupling CO₂.

Plain Language Summary Climate sensitivity, defined as surface temperature increase to doubling of carbon dioxide (CO₂) concentration, is a broadly used metric of anthropogenic climate change. However, it has spanned a wide range for decades due to the uncertainty in radiative forcing and feedback. The time evolution in radiative feedback, for example, adds challenges for evaluating climate sensitivity via simulations with limited length and for comparing model simulations with observational records. In this study, we investigate how ocean heat uptake influences the time evolution of radiative feedback. More specifically, we quantify the dependence of radiative feedback on regional ocean heat uptake in response to an abrupt increase in CO₂ concentration. Results show that the surface warming due to weakened ocean heat uptake over the Southern Ocean decades after CO₂ increase is not locally confined, but has far-field impacts on tropical clouds via remote influences on sea surface temperature and atmospheric stability in the tropics. The tropical sea surface temperature patterns have been shown to be key for understanding transient evolution of radiative feedbacks in previous studies; our findings further suggest that Southern Ocean heat uptake could be a potential root cause for these evolutions.

1. Introduction

Radiative feedbacks describe the efficiency by which the Earth system amplifies or damps out radiative forcings such as increased greenhouse gases. Studies have long shown that the amplitudes of radiative feedbacks vary across models (Charney et al., 1979), largely accounting for the intermodel spread of global warming projections (Knutti et al., 2017). Recent studies have suggested that radiative feedbacks vary with time in historical and increasing carbon dioxide (CO₂) simulations, leading to challenges for predicting transient and equilibrium climate sensitivities (Andrews et al., 2015; Gregory & Andrews, 2016). A mechanism named “pattern effect” has been proposed to account for aspects of both the intermodel spread and the time dependence of radiative feedbacks (Stevens et al., 2016). Pattern effects refer to ways in which regional spatial patterns of sea surface temperature (SST) affect radiative fluxes at the top-of-atmosphere (TOA), thus modulating the feedbacks. A detailed mechanistic understanding of pattern effects is an essential prerequisite for extrapolating future climate sensitivity from short-term transient observations.

Two somewhat different lines of argument have recently emerged. The warming contrast between the West Pacific and other regions has been identified as a key factor influencing the radiative feedbacks via modification of the lower-tropospheric stability and low cloud cover (Ceppi & Gregory, 2019; Dong et al., 2019; Zhou et al., 2017). On the other hand, the spatial pattern of ocean heat uptake (OHU) has also been shown to have a strong effect on radiative feedbacks, with emphasis on the time-evolving relative magnitudes of tropical and extratropical OHU (Kang & Xie, 2014; Rose et al., 2014; Rose & Rayborn, 2016; Rugenstein et al., 2016; Winton et al., 2010). While the SST and OHU perspectives offer seemingly competing explanations for varying radiative feedbacks, some studies have linked the two perspectives by suggesting that the SST patterns on which the feedbacks depend can be driven by OHU patterns (Haugstad et al., 2017; Rugenstein et al., 2016). However, few studies have provided a detailed quantitative attribution of the contribution of regional OHU to pattern effects and time-evolving feedbacks.

The goal of this study is to quantify the influence of time-evolving regional OHU on global SST patterns and radiative feedbacks in response to an abrupt CO₂ increase. Our attribution is based on the linearity of the coupled climate, in which the radiative responses can be considered as the additive contribution from different types of forcings (Section 2.1). The contribution from transient OHU can be evaluated through a Green's Function approach, which attributes the local and far-field impacts of spatially localized OHU (Section 2.2). The attribution of the time-evolving radiative feedback reveals the dominant role of heat uptake over the Southern Ocean, which modifies time-evolution of SST patterns, and in turn influences changes in radiative feedbacks (Section 3). Possible causes for intermodel spread of OHU and their implications on uncertainties of time-evolving radiative feedback are discussed in Section 4.

2. Data and Method

2.1. Linearity of the Coupled Climate

To evaluate the OHU in affecting transient atmospheric and surface responses to CO₂ increase in the coupled climate system, we consider OHU as a forcing (i.e., heat sink/source) to the atmosphere and surface, consistent with previous studies (Rose & Rayborn, 2016; Winton et al., 2010). The linearity of the coupled climate is demonstrated by the additive contribution from different types of forcing (Boer & Yu, 2003; Marvel et al., 2016). In the case of transient responses forced by an abrupt quadrupling of CO₂ (abrupt4 × CO₂) in a coupled climate, one can partition the atmospheric and surface responses in each grid cell i (ΔX_i) into two components. One is the equilibrium responses to time-invariant CO₂ quadrupling without changes in OHU ($\Delta X_{i,\text{CO}_2}$), and the other is the contribution from time-evolving OHU ($\Delta X_{i,\text{OHU}}(t)$), with $\varepsilon(t)$ indicating the residuals, as shown in Equation 1.

$$\Delta X_i(t) = \Delta X_{i,\text{CO}_2} + \Delta X_{i,\text{OHU}}(t) + \varepsilon(t). \quad (1)$$

$\Delta X_i(t)$ is calculated by subtracting the time-mean climatology under preindustrial conditions (piControl) from the transient, 150-years abrupt4 × CO₂ simulation in the fully coupled model CESM1 (CAM5.1, FV2). $\Delta X_{i,\text{CO}_2}$ and $\Delta X_{i,\text{OHU}}(t)$ are individually evaluated in the atmosphere model CAM5 coupled with a non-dynamical slab-ocean. The former is the equilibrium responses in abrupt4 × CO₂ simulation relative to piControl condition, indicating the influences from quadrupling of CO₂ on the atmosphere and surface, without changes in OHU. The latter, representing the equilibrium responses on the atmosphere and surface to time-evolving OHU, is evaluated through a suite of simulations, with each being forced by a localized surface heat flux (Section 2.2). Note that a 7-years low-pass Butterworth digital filter is applied to all the variables to remove the high-frequency variability.

The linearity of the coupled climate is evaluated in Figures 1a and 1b. The time evolution of global-mean anomalous TS (ΔTS) and net downward TOA radiation (ΔR_{net}) of abrupt4 × CO₂ simulation in CESM can be reconstructed by the additive contribution from CO₂ quadrupling and from time-evolving OHU, with the residual being around 1 K for ΔTS and 1 (W / m²) for ΔR_{net} in the first few years and remaining small after that. The residual can be attributed to three main reasons. First, the potential nonlinearities of the coupled climate. For example, responses of sea ice extent to a particular amount of warming could vary, depending

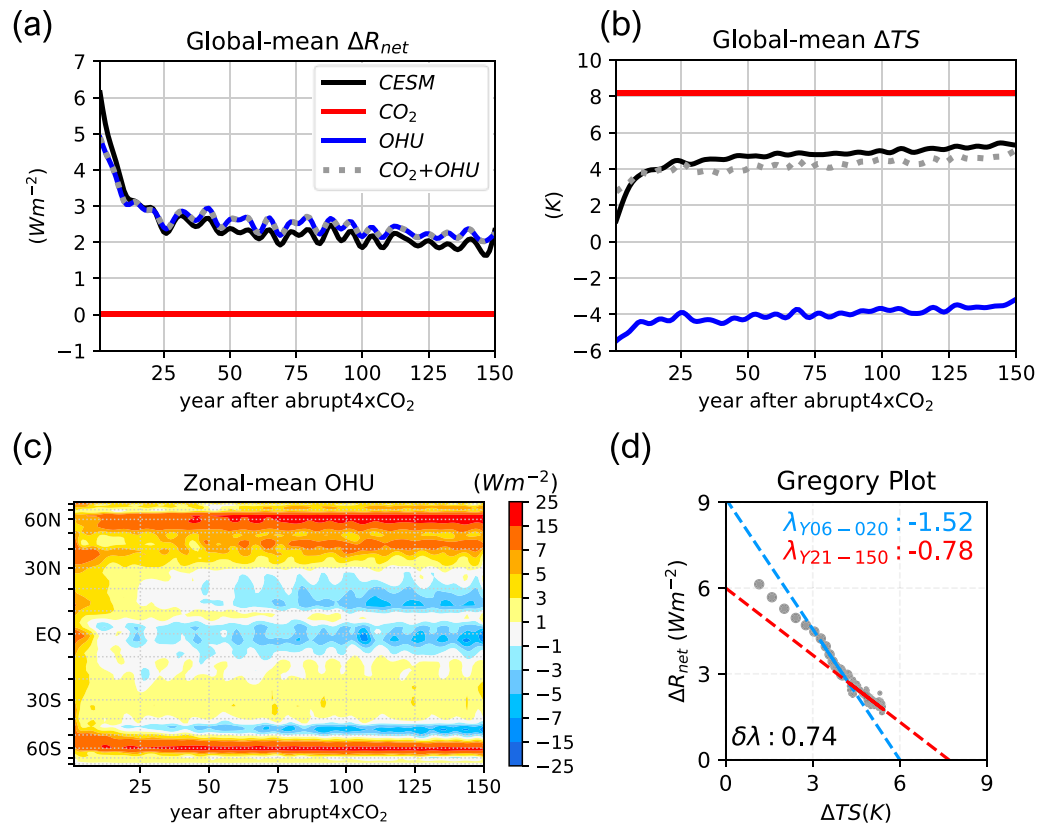


Figure 1. Global-mean (a) ΔR_{net} and (b) ΔTS in CESM (black). The red lines indicate the equilibrium responses in the slab-ocean model. The blue lines are the Green's Function reconstructed responses with transient OHU (Equation 4). The dashed gray lines are the summation of the red and blue lines. (c) Zonal-mean OHU in CESM (positive down). (d) Scatterplot of global-mean ΔR_{net} and ΔTS in CESM (Gregory et al., 2004). OHU, ocean heat uptake.

on multiple thresholds of temperature (Eisenman & Wettlaufer, 2009; Garbe et al., 2020). The nonlinear behavior of the sea ice extent can affect radiative responses through changes in surface albedo, lapse-rate, and water vapor (Lu et al., 2020; Winton, 2008). Second, the climate responses independent from OHU, such as the responses to transient warming/cooling over land and over ice-covered regions. Third, the potential climate noise and the impacts from internal variability in the simulations.

2.2. Evaluating the Contribution of Transient OHU via a Green's Function Approach

To quantify the contribution of transient OHU on atmospheric and surface responses (i.e., $\Delta X_{i,\text{OHU}}(t)$ in Equation 1), we first calculate the time evolution of OHU (Figure 1c), and evaluate its influences via the Green's Function matrix G (Equation 2).

$$G = \begin{pmatrix} \frac{\partial X_1}{\partial \text{OHU}_1} & \dots & \frac{\partial X_1}{\partial \text{OHU}_n} \\ \vdots & \ddots & \vdots \\ \frac{\partial X_m}{\partial \text{OHU}_1} & \dots & \frac{\partial X_m}{\partial \text{OHU}_n} \end{pmatrix}. \quad (2)$$

The form of $\partial X_i / \partial \text{OHU}_j$ indicates the dependence of climate responses on gridded OHU and can be used to evaluate the influences of OHU. The subscript i (j) goes from 1 to m (n), which is the total number of global (oceanic) grid points. G is derived from 108 pairs of simulations, with each being forced with ocean q-flux patches that jointly cover all the open ocean (Figure S1; see Text S1 and F. Liu et al. (2018) for detailed

experimental design). For each grid cell i , the response of X per unit change in OHU at grid j can be determined as follows:

$$\frac{\partial X_i}{\partial \text{OHU}_j} = \frac{\sum_p \text{OHU}'_j \left(\frac{X'_i}{\text{OHU}'_p} \frac{a_j}{a_p} \right)}{\sum_p \text{OHU}'_j}. \quad (3)$$

X'_i is the linear component of the equilibrium response of X at local grid i for each patch. It is first divided by the area-weighted averaged OHU anomaly over the patch p (OHU'_p), and normalized by the ratio of area (a_j / a_p), where a_j is the surface area of the grid box j inside the patch p , and a_p is the total ocean area of the patch p . $\left(\left(X'_i / \text{OHU}'_p \right) \left(a_j / a_p \right) \right)$ accounts for the response of X at grid i to OHU change at grid j within a certain patch p . Since each ocean grid box is covered by multiple overlapping patches, $\partial X_i / \partial \text{OHU}_j$ can be determined by weighting $\left(\left(X'_i / \text{OHU}'_p \right) \left(a_j / a_p \right) \right)$ of all the overlapping patches based on the strength of the OHU anomaly. The derivation of G follows the method in Dong et al. (2019), except that the simulations used in Dong et al. (2019) are a suite of “prescribed SST” simulations, while we used a suite of “prescribed ocean q-flux” simulations.

For any grid cell i , the response of atmospheric or surface variable X to large-scale OHU could be approximated by a first order Taylor series with respect to OHU at all grid boxes j .

$$\Delta X_{i,\text{OHU}}(t) = \sum_{j=1}^n \frac{\partial X_i}{\partial \text{OHU}_j} \text{OHU}_j(t). \quad (4)$$

By combining Equations 1 and 4, the atmospheric or surface responses in CESM can be reconstructed as follows:

$$\Delta X_i(t) = \Delta X_{i,\text{CO}_2} + \sum_{j=1}^n \frac{\partial X_i}{\partial \text{OHU}_j} \text{OHU}_j(t) + \varepsilon(t). \quad (5)$$

3. Results

3.1. Attribute the Radiative Feedback Evolution to Regional OHU

Figure 1d illustrates the evolution of ΔR_{net} and ΔTS in the form of a Gregory plot (Gregory et al., 2004). The radiative feedback parameter λ , calculated as the regression slope of ΔR_{net} against global-mean ΔTS , evolves from $-1.52 \text{ W/m}^2\text{K}$ in year 6–20 to $-0.78 \text{ W/m}^2\text{K}$ in year 21–150 in CESM. To quantify the transient increase of effective climate sensitivity, we define a feedback increment $\delta\lambda$ as

$$\delta\lambda = \frac{d(\overline{\Delta R_{\text{net}}})}{d(\overline{\Delta TS})} \Big|_{Y21-150} - \frac{d(\overline{\Delta R_{\text{net}}})}{d(\overline{\Delta TS})} \Big|_{Y6-20}, \quad (6)$$

where overbars indicate global mean. Accordingly, the time-evolving patterns of surface warming and estimated inversion strength (EIS; Wood & Bretherton, 2006) can be expressed as follows.

$$\delta TS = \frac{d(\overline{\Delta TS})}{d(\overline{\Delta TS})} \Big|_{Y21-150} - \frac{d(\overline{\Delta TS})}{d(\overline{\Delta TS})} \Big|_{Y6-20}, \quad (7)$$

$$\delta EIS = \frac{d(\overline{\Delta EIS})}{d(\overline{\Delta TS})} \Big|_{Y21-150} - \frac{d(\overline{\Delta EIS})}{d(\overline{\Delta TS})} \Big|_{Y6-20}. \quad (8)$$

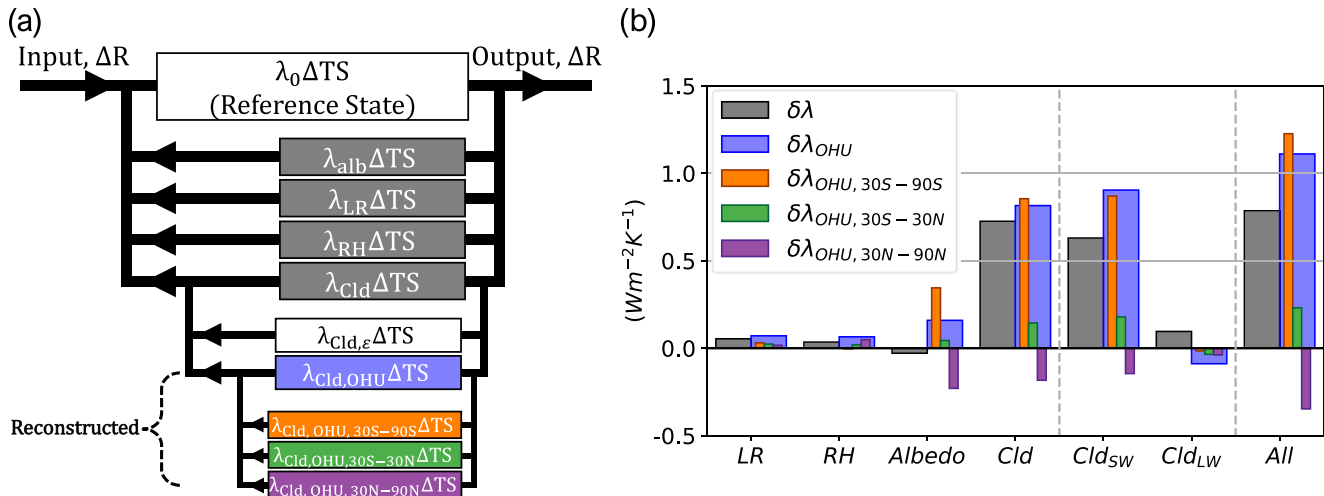


Figure 2. (a) Schematic diagram of the decomposition of net radiative feedback (λ), modified from Roe (2009). (b) Decomposition of the increase in net radiative feedback ($\delta\lambda$).

The first five years are excluded for better comparison with reconstructed radiative feedbacks from Green's Function. The scatterplot in Figure 1d indicates radiative feedback change after year 5. We assume that the response of the coupled climate model during the first few years after abrupt CO₂ quadrupling are dominated by land-atmosphere interactions unrelated to OHU. Note that whether the first five years being excluded or not results in consistent conclusions (Figures S2 and S3). The separation at ~ 20 years distinguishes between the fast and slow components of climate responses (Geoffroy et al., 2013; Held et al., 2010). To understand the time dependence of λ , we decompose ΔR_{net} threefold, indicated by the three loops of Figure 2a. In the first loop, ΔR_{net} is decomposed into radiative anomalies that are related to changes in Planck emission (ΔR_{plk}), surface albedo (ΔR_{alb}), lapse-rate (ΔR_{LR}), relative humidity (ΔR_{RH}), and clouds (ΔR_{Cld}). The first loop of decomposition is done through radiative kernels method (Held & Shell, 2012; Soden et al., 2008), with the kernels calculated with CAM5 (Pendergrass et al., 2018).

$$\Delta R_{net} = \Delta R_{plk} + \Delta R_{alb} + \Delta R_{LR} + \Delta R_{RH} + \Delta R_{Cld}. \quad (9)$$

Planck emission is considered as a property of the blackbody reference state here, in which the climate adjusts to radiative forcing only by changing ΔTS , with an efficiency of λ_0 . Changes in variables other than ΔTS (e.g., albedo, lapse-rate, water vapor, and clouds) amplify or dampen ΔR_{net} , leading to further changes in ΔTS (Figure 2a). The second loop of decomposition is based on the linearity of the climate system (Equation 1), where each radiative anomaly can be further decomposed into two parts: One from the equilibrium responses to CO₂ quadrupling and the other excited by transient OHU. Take ΔR_{Cld} for example,

$$\Delta R_{Cld}(t) = \Delta R_{Cld,CO_2} + \Delta R_{Cld,OHU}(t) + \varepsilon(t). \quad (10)$$

Since the equilibrium responses to CO₂ quadrupling is time-invariant, the radiative feedback in CESM can be simply reconstructed by the Green's Function with transient global OHU, along with potential residuals. The third loop of decomposition attributes the Green's Function reconstruction from global OHU to regional OHU, which can be done by specifying the integration area in Equation 4. Taking $\Delta R_{Cld,OHU}$, for example, here we divide it into three components: The reconstruction with regional OHU over 30°S – 90°S (Southern Hemisphere extratropics), 30°S – 30°N (tropics), and 30°N – 90°N (Northern Hemisphere extratropics):

$$\Delta R_{Cld,OHU}(t) = \Delta R_{Cld,OHU,30S-90S}(t) + \Delta R_{Cld,OHU,30S-30N}(t) + \Delta R_{Cld,OHU,30N-90N}(t). \quad (11)$$

The full decomposition is illustrated in Figure 2a. Note that each radiative feedback contributes to part of the TOA flux variation by scaling with global-mean ΔTS , with the ΔTS simultaneously being affected by

multiple radiative feedbacks. This feature allows us to linearly attribute the net radiative feedback to regional OHU by decomposing radiative fluxes only (Equations 9–11), as done in previous studies (Roe, 2009; Rose & Rayborn, 2016).

Figure 2b shows the decomposition of $\delta\lambda$. The increase in λ can be mostly attributed to the increase in net cloud feedback, especially the cloud's effect on the shortwave radiation, consistent with previous studies (Andrews et al., 2015; Cesspi & Gregory, 2017). Also, the increase in cloud feedback can be reconstructed by the Green's Function with transient OHU, albeit with stronger magnitude (the overestimation is discussed in Section 3.2). The shift toward more positive net cloud feedback arises predominantly from OHU in 30°S–90°S ($\delta\lambda_{\text{Cld}, \text{OHU}, 30^{\circ}\text{S}-90^{\circ}\text{S}}$), as shown by the orange bar for the cloud feedback in Figure 2b. To conclude, 30°S–90°S OHU has the dominant contribution to the increase in cloud feedback and thus the increase in λ (i.e., increase in transient climate sensitivity).

3.2. Influences of Southern Ocean Heat Uptake on Cloud Feedback Change

Figures 3a–3c show the spatial pattern of the increase in cloud feedback and the dominant contribution of 30°S–90°S OHU. The increase in cloud feedback (Figure 3a) can be reconstructed by the Green's Function (Figure 3b), which is mostly attributed to the transient OHU in 30°S–90°S (Figure 3c). Further analysis shows that 51% of the $\delta\lambda_{\text{Cld}, \text{OHU}, 30^{\circ}\text{S}-90^{\circ}\text{S}}$ arises from tropical (30°S–30°N) cloud changes, implying a strong remote impact. Another 38% arises from local cloud changes in 30°S–90°S (Figure 3c). We propose the following physical processes through which 30°S–90°S OHU gives rise to increasingly positive local and remote cloud feedbacks:

- Local and remote influence of OHU on SST: During the first few years after quadrupling CO₂, positive (downward) OHU is relatively uniform (Figure 1c). The 30°S–90°S averaged OHU weakens throughout the 150-years simulation. Specifically, it weakens by 0.7 W / m² per 1 K global-mean surface temperature increase in 6–20 years; this OHU weakening becomes stronger in 21–150 years as it decreases by 0.9 W / m² per 1 K global-mean surface temperature increase (Figure S4). The stronger weakening tendency of 30°S–90°S OHU in the late period leads to the increasingly enhanced southern hemisphere (SH) surface warming relative to the global mean. Based on the Green's Function reconstruction, the surface warming induced by the stronger decrease in 30°S–90°S OHU is not confined to the Southern Ocean, but also extends to the subtropics via eastern basins (Figure 3f). This local and remote SH surface warming pattern due to 30°S–90°S OHU is also found in CESM (albeit with weaker magnitude; Figure 3d), suggesting similar mechanisms operate in a fully coupled climate. While the teleconnection mechanism needs further investigation, our findings are consistent with previous studies suggesting that extratropical OHU can affect tropical SST by generating an anomalous cross-equatorial Hadley Cell, which modifies the trade winds strength and further leads to tropical SST change through wind-evaporation-SST (WES) feedback (Hwang et al., 2017; Kang et al., 2018; Xie et al., 2010).
- Lower-tropospheric stability (LTS) determined by SST pattern: In both the Southern Ocean and the tropics, the evolution of LTS is influenced by δTS , but in different ways. Locally over the Southern Ocean, increasingly enhanced surface warming (positive δTS) destabilizes the lower troposphere (which we quantify through negative δEIS ; Figure 3g). In tropics on the other hand, since tropospheric temperatures are strongly coupled to SST in the West Pacific (WP) convective regions according to the weak temperature gradient approximation (Sobel et al., 2002), LTS is largely determined by the surface warming contrast between convective and nonconvective regions. We find that $\delta\text{TS}_{\text{OHU}, 30^{\circ}\text{S}-90^{\circ}\text{S}}$ in the Southeastern Pacific is more positive than in the WP convective region (gray box in Figure 3f), which explains the destabilization of the nonconvective subtropical regions (Figure 3i). Significantly, we find consistent patterns of negative subtropical δEIS and $\delta\text{EIS}_{\text{OHU}, 30^{\circ}\text{S}-90^{\circ}\text{S}}$, strongly suggesting a remote effect from Southern Ocean heat uptake on tropical stability.
- Changes in cloud feedback linked to stability changes and other factors: The decrease in tropospheric stability, either locally or remotely triggered by 30°S–90°S OHU, acts to decrease the low cloud amount, since a weaker inversion is less efficient in trapping moisture in the boundary layer (Wood & Bretherton, 2006). The decrease in low cloud amount further leads to an increase in net cloud feedback by keeping more shortwave radiation in the climate system (Figure 3c).

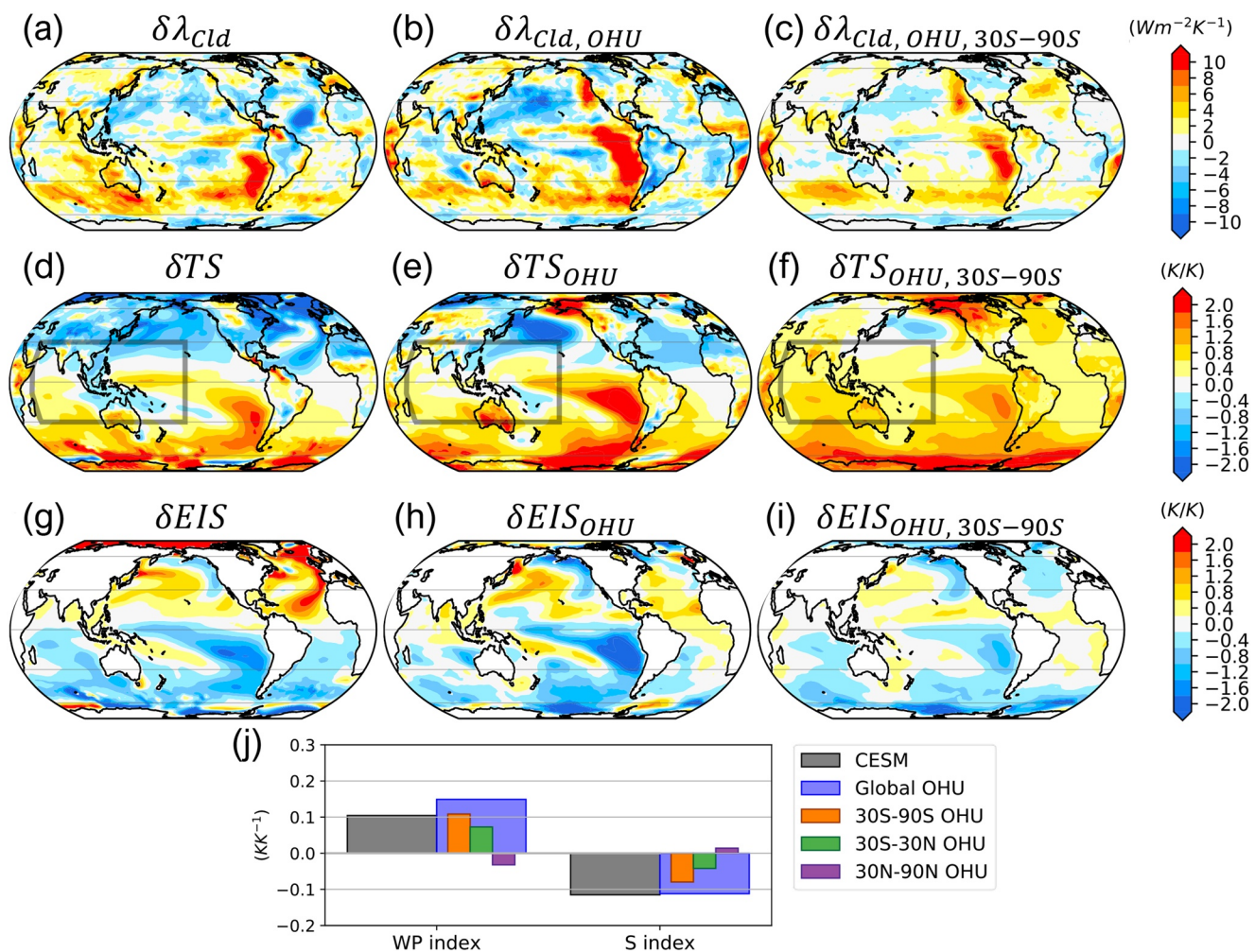


Figure 3. (a) $\delta\lambda_{Cld}$ pattern in CESM. (b) $\delta\lambda_{Cld}$ pattern reconstructed by the Green's Function with global OHU evolution. (c) $\delta\lambda_{Cld}$ pattern reconstructed by the Green's Function with OHU only in $30^{\circ}\text{S} - 90^{\circ}\text{S}$. (d–f) Same as (a, b, c), but for evolution of surface temperature (δTS). (g–i) Same as (a, b, c), but for evolution of EIS (δEIS). (j) WP index and S index from the model output (black), from the Green's Function reconstruction (blue), and their attribution to regional OHU. OHU, ocean heat uptake.

In addition to the low cloud amount change discussed above, cloud albedo can also modify the strength of the cloud feedback. Area-weighted average of liquid water path (LWP) over $30^{\circ}\text{S} - 90^{\circ}\text{S}$ increases by 9% in years 6–20 while local SST evolves from 278 to 279 K, causing phase changes in low-level clouds. In contrast, LWP holds nearly constant in the following 130 years while local SST is still rising, from 279 to 282 K. The halt of increasing LWP in the late period results in a more positive shortwave cloud feedback (Figure S5), as the increase in LWP accounts for larger cloud albedo (McCoy et al., 2014; Zelinka et al., 2012). The LWP evolution in Southeastern Pacific also leads to more positive cloud feedback, while the cause for decreasing LWP might be related with the decrease in cloud amount (their time evolution is positively correlated with a coefficient of 0.71) as the local SST is too high for phase changes (Figure S5).

It is worth noting that the tropical δTS and δEIS in response to quadrupling CO_2 are largely influenced remotely by Southern Ocean heat uptake, rather than local OHU evolution in tropics. Figure 3j quantifies the Green's Function reconstruction with transient OHU over three different latitudinal bands on the tropical δTS and δEIS . First, we define WP index as the area-weighted averaged oceanic δTS in $50^{\circ}\text{S} - 50^{\circ}\text{N}$ outside the WP minus that inside the WP. The WP region is defined within $30^{\circ}\text{S} - 30^{\circ}\text{N}$, $50^{\circ}\text{E} - 160^{\circ}\text{W}$ (shown as the gray box in Figures 3d–3f), following Dong et al. (2019). Results show that the positive WP index in CESM is mostly due to the OHU evolution in $30^{\circ}\text{S} - 90^{\circ}\text{S}$. Consistently, S index, defined as area-weighted

averaged $50^{\circ}\text{S} - 50^{\circ}\text{N}$ oceanic δEIS , following Ceppi and Gregory (2017, 2019), can also be attributed to OHU in SH extratropics. The remote impact from extratropical OHU to tropical SST pattern bridges the two aforementioned hypotheses for the time-evolving radiative feedbacks: One emphasizes the warming contrast between the WP and other regions (Dong et al., 2019), and the other emphasizes the different efficacy between tropical and extratropical OHU (Rose & Rayborn, 2016; Winton et al., 2010). Through its remote effects on tropical SST patterns and lower-tropospheric stability, heat uptake in the Southern Ocean can explain most of the change in net radiative feedback in CESM (Figure 2b).

In this work, we show that Green's Function approach can linearly reconstruct the time-evolution of cloud feedback and SST pattern, allowing for a detailed attribution to regional OHU. However, the residuals of this reconstruction deserve mentioning here (Figure S6). As discussed in Section 2.1, the residuals result from the nonlinear response to OHU, the component independent from OHU, and the potential climate noise. Here we suggest that the nonlinear responses to OHU might partly explain the residuals of δTS and $\delta\lambda_{\text{Cld}}$, especially the overestimation in eastern Pacific. Compared to the linear responses, nonlinear responses are less sensitive to the location of the q-flux (Figure S7). For a certain amount of surface warming/cooling, no matter where it is imposed, both the global-mean and spatial pattern of the nonlinear responses are similar—consistently showing the cooling over eastern Pacific. The cooling effect from the nonlinearity, however, is expected to decrease as warming continues and sea ice retreats, since it is mainly driven by the presence of sea ice (Liu et al., 2020). As sea ice significantly retreats few decades after CO_2 quadrupling (not shown), we may infer that the nonlinearity is more prominent during the early period, causing warm bias in the first few years (Figure 1b). This would also contribute to the weaker warming tendency in the early period, especially in eastern Pacific, and hence the over-estimation of increasingly enhanced surface warming (δTS) and net cloud feedback increase ($\delta\lambda_{\text{Cld}}$) over there (cf. Figures 3a–3b and 3d–3e).

4. Summary and Discussion

Cloud feedback has remained the primary source of model uncertainty in the global warming projection for decades (Soden & Held, 2006; Zelinka et al., 2017), with the subtropical low-level clouds contributing most to the uncertainty (Bony & Dufresne, 2005; Myers & Norris, 2016). Previous studies have demonstrated that the stronger (weaker) warming in the West Pacific relative to other regions would lead to an (a) increase (decrease) in subtropical low-level clouds, accounting for less (more) sensitive radiative feedbacks (Andrews & Webb, 2018; Dong et al., 2019; Gregory & Andrews, 2016; Zhou et al., 2016). Question remains as to the ultimate causes of the time-evolution of these radiatively important tropical SST patterns.

In this work, we highlight that the evolving tropical SST pattern is driven remotely by variations in Southern Ocean heat uptake. This effect is most prominent in the Southeast subtropical Pacific, where the increasingly enhanced warming is driven by slowly weakening Southern Ocean heat uptake, and leads to low-cloud loss and a more positive net cloud feedback. Rose et al. (2014) and Rugenstein et al. (2016) have suggested OHU being the root cause of evolution of radiative feedbacks. Here, we corroborate this notion and further highlight the critical role of the Southern Ocean, which is likely to be the root cause of the evolution of tropical SST patterns and cloud radiative feedbacks in abrupt4 $\times \text{CO}_2$ simulation in CESM.

In contrary to the OHU in SH extratropics, the OHU in the NH extratropics weakens in the first 20 years and strengthens in the following 130 years (Figure S4). The strengthening of the $30^{\circ}\text{N} - 90^{\circ}\text{N}$ OHU leads to a cooler NH relative to the global-mean warming decades after quadrupling of CO_2 . The cooler NH projects onto a more stable troposphere and a more negative cloud feedback, which is mostly confined to the NH and is especially robust in the Atlantic Ocean basin (Figure S8), accounting for the more negative cloud feedback and decrease in $\delta\lambda$ shown in Figure 2b.

Given the large CMIP5 intermodel spread of OHU in both hemispheres, it is worth noting that the contrasting evolution between NH and SH extratropics in the CESM might not hold for individual CMIP5 models. First, the magnitudes of the overall decline in Southern Ocean heat uptake vary among models (Figure S4). An implication of the remote influence demonstrated in this study is that uncertainty in the evolution of subtropical low-level clouds and cloud feedbacks could be partly traced to uncertainty in the evolution of Southern Ocean heat uptake, as suggested by Rose and Rayborn (2016). Second, the time evolution of NH extratropical OHU is strongly model dependent—some models project a weakening of OHU decades after

quadrupling of CO₂ while some project a strengthening (Figure S4). The NH surface temperature and cloud feedback evolution also appear to be less robust among models (Ceppi & Gregory, 2017; Lin et al., 2019). In contrast to OHU over Southern Ocean that is mostly determined by the mean state of the ocean (Armour et al., 2016; W. Liu et al., 2018; Manabe et al., 1990; Marshall et al., 2014), one of the key factors determining OHU in the NH is the variations of Atlantic Meridional Overturning Circulation (AMOC; Chen & Tung, 2018; Kostov et al., 2014). The time evolution of AMOC intensity, including the weakening within decades after increasing CO₂ and the recovery in timescales of hundreds of years (Cheng et al., 2013; Stouffer et al., 2006), have been shown to modulate radiative feedbacks (Caesar et al., 2020; Lin et al., 2019; Trossman et al., 2016). Focusing on a single model (CESM), our work highlights the critical role of the Southern Ocean. For intermodel spread or for models with more apparent AMOC recovery, OHU over Southern Ocean and North Atlantic could both be important for the transient increase of effective climate sensitivity. We suggest the base climate oceanic circulation may thus have an important influence on climate sensitivity (He et al., 2017; Winton et al., 2014) via affecting the evolution of ocean heat uptake, which then alters cloud radiative effects both locally and remotely.

Data Availability Statement

All CMIP data can be downloaded from the ESGF at <https://esgf-node.llnl.gov/projects/esgf-llnl/>. This research was undertaken with the assistance of resources and services from the National Energy Research Scientific Computing Center (NERSC), supported by the U.S. Government. Processed data to support the analysis are published at <https://doi.org/10.5281/zenodo.4588073>.

Acknowledgments

The authors acknowledge the World Climate Research Program's Working Group on Coupled Modeling, which is responsible for CMIP, and we thank the climate modeling groups (Table S1) for producing and making available their model output. For CMIP, the U.S. Department of Energy's Program for Climate Model Diagnosis and Intercomparison provided coordinating support and led development of software infrastructure in partnership with the Global Organization for Earth System Science Portals. Y. J. Lin and Y. T. Hwang were supported by Ministry of Science and Technology of Taiwan (MOST 110-2628-M-002-002-). J. Lu was supported by the U.S. Department of Energy Office of Science Biological and Environmental Research as part of the Regional and Global Modeling and Analysis program. F. Liu was supported by the National Natural Science Foundation of China (NSFC; 41906002 and 91858210). B. E. J. Rose was supported by NSF grant AGS-1455071.

References

- Andrews, T., Gregory, J. M., & Webb, M. J. (2015). The dependence of radiative forcing and feedback on evolving patterns of surface temperature change in climate models. *Journal of Climate*, 28(4), 1630–1648. <https://doi.org/10.1175/Jcli-D-14-00545.1>
- Andrews, T., & Webb, M. J. (2018). The dependence of global cloud and lapse rate feedbacks on the spatial structure of tropical Pacific warming. *Journal of Climate*, 31(2), 641–654. <https://doi.org/10.1175/jcli-d-17-0087.1>
- Armour, K. C., Marshall, J., Scott, J. R., Donohoe, A., & Newsom, E. R. (2016). Southern Ocean warming delayed by circumpolar upwelling and equatorward transport. *Nature Geoscience*, 9(7), 549–554. <https://doi.org/10.1038/ngeo2731>
- Boer, G., & Yu, B. (2003). Climate sensitivity and response. *Climate Dynamics*, 20(4), 415–429. <https://doi.org/10.1007/s00382-002-0283-3>
- Bony, S., & Dufresne, J. L. (2005). Marine boundary layer clouds at the heart of tropical cloud feedback uncertainties in climate models. *Geophysical Research Letters*, 32(20). <https://doi.org/10.1029/2005gl023851>
- Caesar, L., Rahmstorf, S., & Feulner, G. (2020). On the relationship between Atlantic meridional overturning circulation slowdown and global surface warming. *Environmental Research Letters*, 15(2), 024003. <https://doi.org/10.1088/1748-9326/ab63e3>
- Ceppi, P., & Gregory, J. M. (2017). Relationship of tropospheric stability to climate sensitivity and Earth's observed radiation budget. *Proceedings of the National Academy of Sciences of the United States of America*, 114, 13126–13131. <https://doi.org/10.1073/pnas.1714308114>
- Ceppi, P., & Gregory, J. M. (2019). A refined model for the Earth's global energy balance. *Climate Dynamics*, 53, 4781–4797. <https://doi.org/10.1007/s00382-019-04825-x>
- Charney, J. G., Arakawa, A., Baker, D. J., Bolin, B., Dickinson, R. E., Goody, R. M., et al. (1979). *Carbon dioxide and climate: A scientific assessment*. Washington, DC: National Academy of Sciences.
- Chen, X., & Tung, K.-K. (2018). Global surface warming enhanced by weak Atlantic overturning circulation. *Nature*, 559(7714), 387–391. <https://doi.org/10.1038/s41586-018-0320-y>
- Cheng, W., Chiang, J. C. H., & Zhang, D. (2013). Atlantic meridional overturning circulation (AMOC) in CMIP5 models: RCP and historical simulations. *Journal of Climate*, 26(18), 7187–7197. <https://doi.org/10.1175/jcli-d-12-00496.1>
- Dong, Y., Proistosescu, C., Armour, K. C., & Battisti, D. S. (2019). Attributing historical and future evolution of radiative feedbacks to regional warming patterns using a Green's function approach: The preeminence of the Western Pacific. *Journal of Climate*, 32(17), 5471–5491.
- Eisenman, I., & Wettlaufer, J. S. (2009). Nonlinear threshold behavior during the loss of Arctic sea ice. *Proceedings of the National Academy of Sciences*, 106(1), 28–32. <https://doi.org/10.1073/pnas.0806887106>
- Garbe, J., Albrecht, T., Levermann, A., Donges, J. F., & Winkelmann, R. (2020). The hysteresis of the Antarctic ice sheet. *Nature*, 585(7826), 538–544. <https://doi.org/10.1038/s41586-020-2727-5>
- Geoffroy, O., Saint-Martin, D., Bellon, G., Volodire, A., Olivie, D. J. L., & Tytéca, S. (2013). Transient climate response in a two-layer energy-balance model. Part II: Representation of the efficacy of deep-ocean heat uptake and validation for CMIP5 AOGCMs. *Journal of Climate*, 26(6), 1859–1876. <https://doi.org/10.1175/jcli-d-12-00196.1>
- Gregory, J. M., & Andrews, T. (2016). Variation in climate sensitivity and feedback parameters during the historical period. *Geophysical Research Letters*, 43(8), 3911–3920. <https://doi.org/10.1002/2016gl068406>
- Gregory, J. M., Ingram, W., Palmer, M., Jones, G., Stott, P., Thorpe, R., et al. (2004). A new method for diagnosing radiative forcing and climate sensitivity. *Geophysical Research Letters*, 31(3). <https://doi.org/10.1029/2003gl018747>
- Haugstad, A. D., Armour, K. C., Battisti, D. S., & Rose, B. E. J. (2017). Relative roles of surface temperature and climate forcing patterns in the inconstancy of radiative feedbacks. *Geophysical Research Letters*, 44(14), 7455–7463. <https://doi.org/10.1002/2017gl074372>
- He, J., Winton, M., Vecchi, G., Jia, L., & Rugenstein, M. (2017). Transient climate sensitivity depends on base climate ocean circulation. *Journal of Climate*, 30(4), 1493–1504. <https://doi.org/10.1175/jcli-d-16-0581.1>

- Held, I. M., & Shell, K. M. (2012). Using relative humidity as a state variable in climate feedback analysis. *Journal of Climate*, 25(8), 2578–2582. <https://doi.org/10.1175/Jcli-D-11-00721.1>
- Held, I. M., Winton, M., Takahashi, K., Delworth, T., Zeng, F., & Vallis, G. K. (2010). Probing the fast and slow components of global warming by returning abruptly to preindustrial forcing. *Journal of Climate*, 23(9), 2418–2427. <https://doi.org/10.1175/2009jcli3466.1>
- Hwang, Y.-T., Xie, S.-P., Deser, C., & Kang, S. M. (2017). Connecting tropical climate change with Southern Ocean heat uptake. *Geophysical Research Letters*, 44(18), 9449–9457. <https://doi.org/10.1002/2017gl074972>
- Kang, S. M., Park, K., Hwang, Y. T., & Hsiao, W. T. (2018). Contrasting tropical climate response pattern to localized thermal forcing over different ocean basins. *Geophysical Research Letters*, 45(22), 544–612. <https://doi.org/10.1029/2018gl080697>
- Kang, S. M., & Xie, S.-P. (2014). Dependence of climate response on meridional structure of external thermal forcing. *Journal of Climate*, 27(14), 5593–5600. <https://doi.org/10.1175/jcli-d-13-00622.1>
- Knutti, R., Rugenstein, M. A. A., & Hegerl, G. C. (2017). Beyond equilibrium climate sensitivity. *Nature Geoscience*, 10(10), 727–736. <https://doi.org/10.1038/ngeo3017>
- Kostov, Y., Armour, K. C., & Marshall, J. (2014). Impact of the Atlantic meridional overturning circulation on ocean heat storage and transient climate change. *Geophysical Research Letters*, 41(6), 2108–2116. <https://doi.org/10.1002/2013gl058998>
- Lin, Y. J., Hwang, Y. T., Ceppi, P., & Gregory, J. M. (2019). Uncertainty in the evolution of climate feedback traced to the strength of the Atlantic meridional overturning circulation. *Geophysical Research Letters*, 46(21), 12331–12339. <https://doi.org/10.1029/2019gl083084>
- Liu, F., Lu, J., Garuba, O., Leung, L. R., Luo, Y., & Wan, X. (2018). Sensitivity of surface temperature to oceanic forcing via q-flux Green's function experiments. Part I: Linear response function. *Journal of Climate*, 31(9), 3625–3641. <https://doi.org/10.1175/jcli-d-17-0462.1>
- Liu, F., Lu, J., Huang, Y., Leung, L. R., Harrop, B. E., & Luo, Y. (2020). Sensitivity of surface temperature to oceanic forcing via q-flux Green's function experiments. Part III: Asymmetric response to warming and cooling. *Journal of Climate*, 33(4), 1283–1297. <https://doi.org/10.1175/jcli-d-19-0131.1>
- Liu, W., Lu, J., Xie, S.-P., & Fedorov, A. (2018). Southern Ocean heat uptake, redistribution, and storage in a warming climate: The role of meridional overturning circulation. *Journal of Climate*, 31(12), 4727–4743. <https://doi.org/10.1175/jcli-d-17-0761.1>
- Lu, J., Liu, F., Leung, L. R., & Lei, H. (2020). Neutral modes of surface temperature and the optimal ocean thermal forcing for global cooling. *npj Climate and Atmospheric Science*, 3(1), 1–9. <https://doi.org/10.1038/s41612-020-0112-6>
- Manabe, S., Bryan, K., & Spelman, M. J. (1990). Transient response of a global ocean-atmosphere model to a doubling of atmospheric carbon dioxide. *Journal of Physical Oceanography*, 20(5), 722–749. [https://doi.org/10.1175/1520-0485\(1990\)020<0722:troago>2.0.co;2](https://doi.org/10.1175/1520-0485(1990)020<0722:troago>2.0.co;2)
- Marshall, J., Armour, K. C., Scott, J. R., Kostov, Y., Hausmann, U., Ferreira, D., et al. (2014). The ocean's role in polar climate change: Asymmetric Arctic and Antarctic responses to greenhouse gas and ozone forcing. *Philosophical Transactions of the Royal Society A*, 372(2019), 20130040. <https://doi.org/10.1098/rsta.2013.0040>
- Marvel, K., Schmidt, G. A., Miller, R. L., & Nazarenko, L. S. (2016). Implications for climate sensitivity from the response to individual forcings. *Nature Climate Change*, 6(4), 386–389. <https://doi.org/10.1038/nclimate2888>
- Mccoy, D. T., Hartmann, D. L., & Grosvenor, D. P. (2014). Observed Southern Ocean cloud properties and shortwave reflection. Part II: Phase changes and low cloud feedback. *Journal of Climate*, 27(23), 8858–8868. <https://doi.org/10.1175/jcli-d-14-00288.1>
- Myers, T. A., & Norris, J. R. (2016). Reducing the uncertainty in subtropical cloud feedback. *Geophysical Research Letters*, 43(5), 2144–2148. <https://doi.org/10.1002/2015gl067416>
- Pendergrass, A. G., Conley, A., & Vitt, F. M. (2018). Surface and top-of-atmosphere radiative feedback kernels for CESM-CAM5. *Earth System Science Data*, 10(1), 317–324. <https://doi.org/10.5194/essd-10-317-2018>
- Roe, G. (2009). Feedbacks, timescales, and seeing red. *Annual Review of Earth and Planetary Sciences*, 37, 93–115. <https://doi.org/10.1146/annurev.earth.061008.134734>
- Rose, B. E. J., Armour, K. C., Battisti, D. S., Feldl, N., & Koll, D. D. B. (2014). The dependence of transient climate sensitivity and radiative feedbacks on the spatial pattern of ocean heat uptake. *Geophysical Research Letters*, 41(3), 1071–1078. <https://doi.org/10.1002/2013gl058955>
- Rose, B. E. J., & Rayborn, L. (2016). The effects of ocean heat uptake on transient climate sensitivity. *Current Climate Change Reports*, 2(4), 190–201. <https://doi.org/10.1007/s40641-016-0048-4>
- Rugenstein, M. A. A., Caldeira, K., & Knutti, R. (2016). Dependence of global radiative feedbacks on evolving patterns of surface heat fluxes. *Geophysical Research Letters*, 43(18), 9877–9885. <https://doi.org/10.1002/2016gl070907>
- Sobel, A. H., Held, I. M., & Bretherton, C. S. (2002). The ENSO signal in tropical tropospheric temperature. *Journal of Climate*, 15(18), 2702–2706. [https://doi.org/10.1175/1520-0442\(2002\)015<2702:tesitt>2.0.co;2](https://doi.org/10.1175/1520-0442(2002)015<2702:tesitt>2.0.co;2)
- Soden, B. J., & Held, I. M. (2006). An assessment of climate feedbacks in coupled ocean-atmosphere models. *Journal of Climate*, 19(14), 3354–3360. <https://doi.org/10.1175/jcli3799.1>
- Soden, B. J., Held, I. M., Colman, R., Shell, K. M., Kiehl, J. T., & Shields, C. A. (2008). Quantifying climate feedbacks using radiative kernels. *Journal of Climate*, 21(14), 3504–3520. <https://doi.org/10.1175/2007jcli2110.1>
- Stevens, B., Sherwood, S. C., Bony, S., & Webb, M. J. (2016). Prospects for narrowing bounds on Earth's equilibrium climate sensitivity. *Earth's Future*, 4(11), 512–522. <https://doi.org/10.1002/2016ef000376>
- Stouffer, R. J., Yin, J., Gregory, J. M., Dixon, K. W., Spelman, M. J., Hurlin, W., et al. (2006). Investigating the causes of the response of the thermohaline circulation to past and future climate changes. *Journal of Climate*, 19(8), 1365–1387. <https://doi.org/10.1175/jcli3689.1>
- Trossman, D. S., Palter, J. B., Merlis, T. M., Huang, Y., & Xia, Y. (2016). Large-scale ocean circulation-cloud interactions reduce the pace of transient climate change. *Geophysical Research Letters*, 43(8), 3935–3943. <https://doi.org/10.1002/2016gl067931>
- Winton, M. (2008). Sea ice-albedo feedback and nonlinear Arctic climate change. *Arctic Sea Ice Decline: Observations, Projections, Mechanisms, and Implications*, *Geophysical Monograph Series*, 180, 111–131.
- Winton, M., Anderson, W. G., Delworth, T. L., Griffies, S. M., Hurlin, W. J., & Rosati, A. (2014). Has coarse ocean resolution biased simulations of transient climate sensitivity? *Geophysical Research Letters*, 41(23), 8522–8529. <https://doi.org/10.1002/2014gl061523>
- Winton, M., Takahashi, K., & Held, I. M. (2010). Importance of ocean heat uptake efficacy to transient climate change. *Journal of Climate*, 23(9), 2333–2344. <https://doi.org/10.1175/2009jcli3139.1>
- Wood, R., & Bretherton, C. S. (2006). On the relationship between stratiform low cloud cover and lower-tropospheric stability. *Journal of Climate*, 19(24), 6425–6432. <https://doi.org/10.1175/jcli3988.1>
- Xie, S.-P., Deser, C., Vecchi, G. A., Ma, J., Teng, H., & Wittenberg, A. T. (2010). Global warming pattern formation: Sea surface temperature and rainfall. *Journal of Climate*, 23(4), 966–986. <https://doi.org/10.1175/2009jcli3329.1>
- Zelinka, M. D., Klein, S. A., & Hartmann, D. L. (2012). Computing and partitioning cloud feedbacks using cloud property histograms. Part II: Attribution to changes in cloud amount, altitude, and optical depth. *Journal of Climate*, 25(11), 3736–3754. <https://doi.org/10.1175/jcli-d-11-00249.1>

- Zelinka, M. D., Randall, D. A., Webb, M. J., & Klein, S. A. (2017). Clearing clouds of uncertainty. *Nature Climate Change*, 7(10), 674–678. <https://doi.org/10.1038/nclimate3402>
- Zhou, C., Zelinka, M. D., & Klein, S. A. (2016). Impact of decadal cloud variations on the Earth's energy budget. *Nature Geoscience*, 9(12), 871–874. <https://doi.org/10.1038/ngeo2828>
- Zhou, C., Zelinka, M. D., & Klein, S. A. (2017). Analyzing the dependence of global cloud feedback on the spatial pattern of sea surface temperature change with a Green's function approach. *Journal of Advances in Modeling Earth Systems*, 9(5), 2174–2189. <https://doi.org/10.1002/2017ms001096>

Reference From the Supporting Information

- Taylor, K. E., Crucifix, M., Braconnot, P., Hewitt, C. D., Doutriaux, C., Broccoli, A. J., et al. (2007). Estimating shortwave radiative forcing and response in climate models. *Journal of Climate*, 20(11), 2530–2543. <https://doi.org/10.1175/jcli4143.1>



GEOPHYSICAL RESEARCH LETTER

Supporting Information for

The dominant contribution of Southern Ocean heat uptake to time-evolving radiative feedback in CESM

Yuan-Jen Lin¹, Yen-Ting Hwang^{1†}, Jian Lu², Fukai Liu³, and Brian E. J. Rose⁴

¹Department of Atmospheric Sciences, National Taiwan University, Taiwan

²Atmospheric Sciences and Global Change Division, Pacific Northwest National Laboratory, Richland, Washington, USA

³Key Laboratory of Physical Oceanography, Institute for Advanced Ocean Studies, Ocean University of China and Qingdao National Laboratory for Marine Science and Technology, Qingdao, China

⁴Department of Atmospheric and Environmental Sciences, University at Albany, State University of New York, Albany, New York, USA

†Corresponding author: Yen-Ting Hwang (ythwang@ntu.edu.tw)

Contents of this file

Text S1
Figures S1 to S8
Table S1

Text S1. Data of Patches Experiments

108 pairs of simulations are used to build the linear Green's Function (equation (2)), with each pair being forced by two localized surface heat flux (q-flux) anomalies of the same magnitude but opposite signs (Figure S1; Liu et al. (2018)). The model used in this study is Community Earth System Model, version 1.1 (CESM1.1), coupled with a slab ocean model (CESM–SOM), in which the active Community Atmosphere Model, version 5 (CAM5), the Community Land Model, version 4 (CLM4), and the Community Ice Code (CICE) are included with the CESM–SOM. The q-flux patch forcing is designed as a cosine hump:

$$\begin{cases} \pm Q \cos^2\left(\frac{\pi}{2} \frac{\phi - \phi_k}{\phi_w}\right) \cos^2\left(\frac{\pi}{2} \frac{\lambda - \lambda_k}{\lambda_w}\right), & \text{for } -\phi_w \leq \phi - \phi_k \leq \phi_w \text{ and } -\lambda_w \leq \lambda - \lambda_k \leq \lambda_w \\ 0, & \text{otherwise.} \end{cases}$$

where, Q is the peak value of the hump, set to be 12 W m^{-2} , (ϕ_k, λ_k) denotes the latitude and longitude of the center of the patch, $\phi_w = 12^\circ$ and $\lambda_w = 30^\circ$ are the half-widths of the rectangular patch in zonal and meridional directions, respectively. The simulations are integrated for 40 years, and only the last 20 years are used, given that 20 years are needed for slab ocean models to reach an equilibrium state. The anomalies of variable X in each patch experiment (X') are calculated as the 20-years mean of X in response to a q-flux patch (X_{patch}) minus the climatologically mean X in the piControl simulation ($X_{piControl}$):

$$X' = X_{patch} - X_{piControl}$$

The linear and nonlinear components of the anomalies can be estimated as follows:

$$X'_{linear} = \frac{X'_{+Q} - X'_{-Q}}{2};$$

$$X'_{nonlinear} = \frac{X'_{+Q} + X'_{-Q}}{2}.$$

where, the subscript $+Q(-Q)$ indicates the simulation forced with positive (negative) q-flux.

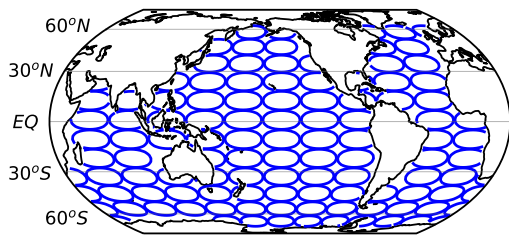


Figure S1. (Reproduction of Figure 1 in Liu et al. (2018), with two more pairs of simulations) Configuration of 108 ocean q-flux perturbation patches, with each being illustrated by the 6 Wm^{-2} contours. Note that the size of the patches is actually larger than the contoured area.

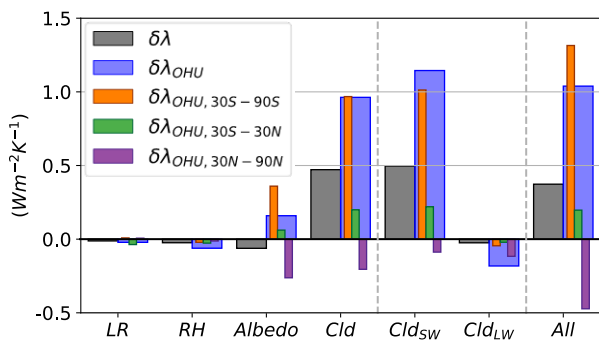


Figure S2. Same as Figure 2b, but with full data (including the first five years).

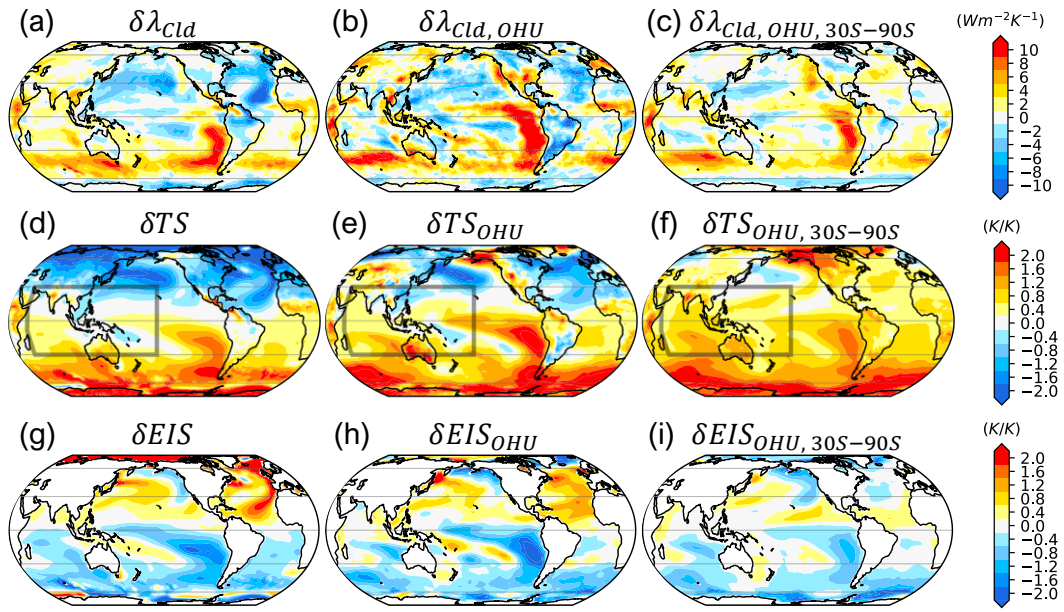


Figure S3. Same as Figure 3, but with full data (including the first five years).

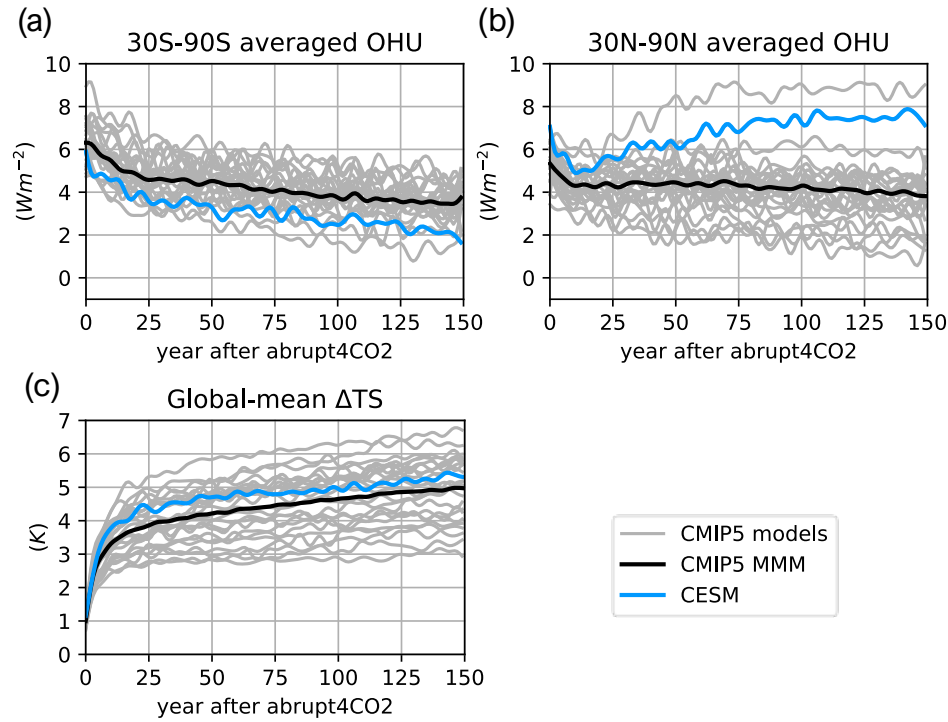


Figure S4. (a) 30S-90S averaged OHU in 24 CMIP5 models (gray), in multimodel mean (black), and in CESM (blue). (b) Same as (a), but for 30N-90N averaged OHU. (c) Same as (a), but for global-mean surface temperature anomaly. The used CMIP5 models are listed in Table S1.

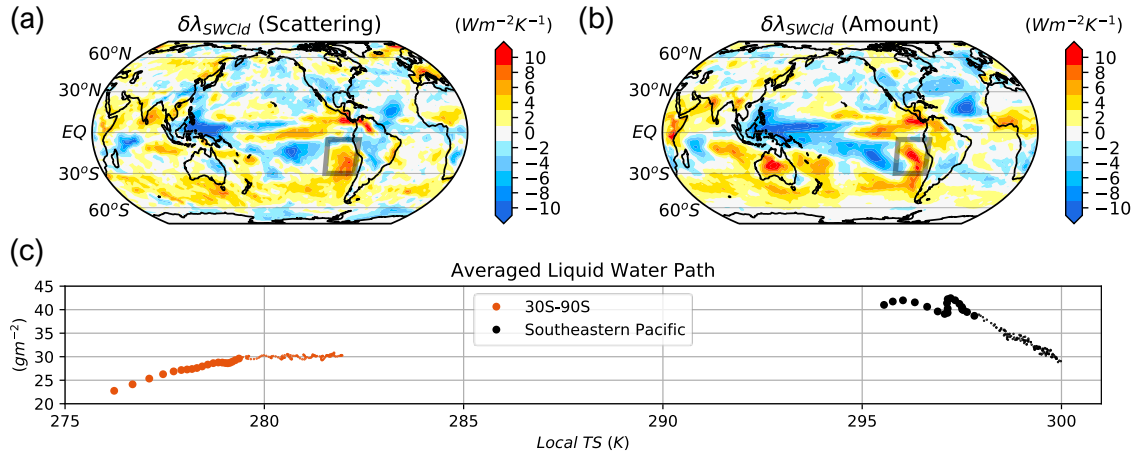


Figure S5. Shortwave cloud feedback changes in CESM due to changes in (a) scattering (b) cloud fraction, determined by the approximate partial radiative perturbation (APRP) method, which estimates shortwave cloud radiative anomalies and their components of cloud amount, scattering, and absorption (Taylor et al., 2007). (c) The evolution of liquid water path in 30S-90S and in Southeastern Pacific (gray box in (a) and (b)).

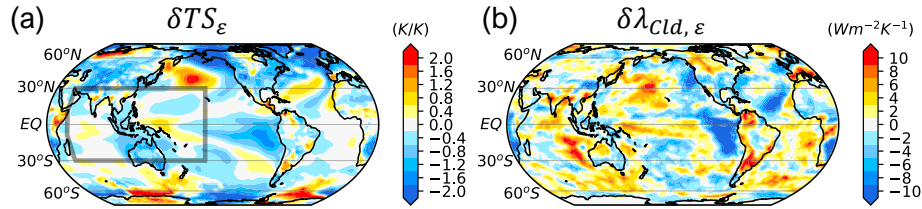


Figure S6. (a) Residuals from the Green's Function reconstruction of the change in surface warming pattern (i.e., the difference between Figure 3d and 3e) (b) Residuals from the Green's Function reconstruction of the change in net cloud feedback (i.e., the difference between Figure 3a and 3b).

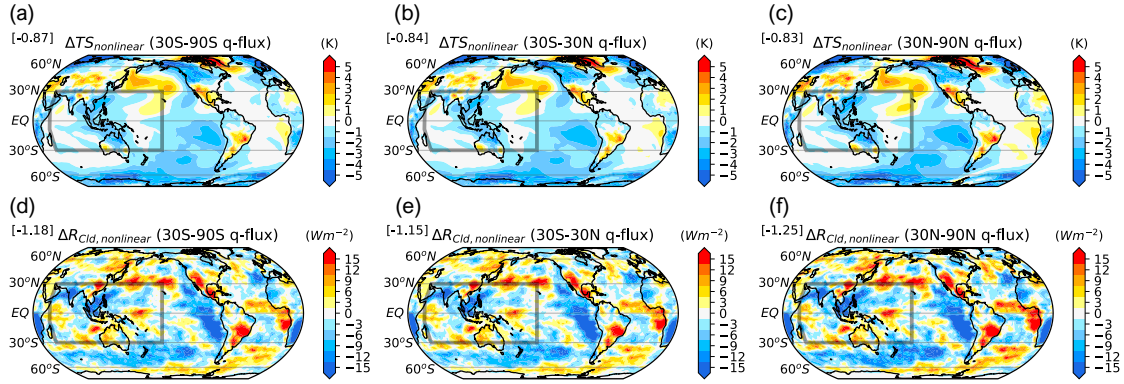


Figure S7. (a, b, c) Nonlinear TS response (i.e., $TS'_{nonlinear}$ in Text S1) to uniform 1 Wm^{-2} warming/cooling over (a) 30S-90S, (b) 30S-30N, and (c) 30N-90N. (d, e, f) Similar to (a, b, c), but for net cloud radiative anomaly. Numbers in the top left corner of each figure denote global-mean values. The responses are normalized by their relative global-sum forcing amplitudes.

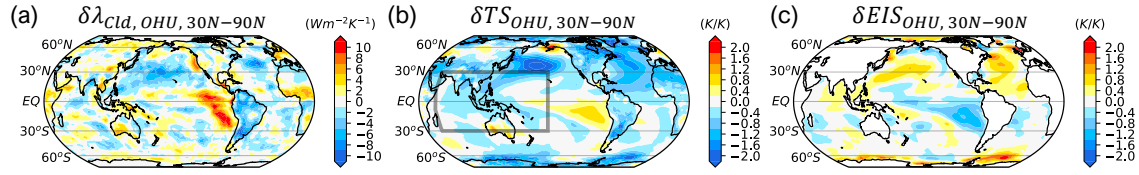


Figure S8. (a) Change in net cloud feedback pattern due to 30N-90N OHU. (b) Change in surface warming pattern due to 30N-90N OHU. (c) Change in EIS pattern due to 30N-90N OHU.

Modeling Center (or Group)	Institute ID	Model Name
Commonwealth Scientific and Industrial Research Organization (CSIRO) and Bureau of Meteorology (BOM), Australia	CSIRO-BOM	ACCESS1.0 ACCESS1.3
Beijing Climate Center, China Meteorological Administration	BCC	BCC-CSM1.1 BCC-CSM1.1(m)
Canadian Centre for Climate Modelling and Analysis	CCCMA	CanESM2
National Center for Atmospheric Research	NCAR	CCSM4
Community Earth System Model Contributors	NSF-DOE-NCAR	CESM1(CAM5.1,FV2)
Centre National de Recherches Météorologiques / Centre Européen de Recherche et Formation Avancée en Calcul Scientifique	CNRM-CERFACS	CNRM-CM5
LASG, Institute of Atmospheric Physics, Chinese Academy of Sciences	LASG-IAP	FGOALS-s2
NOAA Geophysical Fluid Dynamics Laboratory	NOAA GFDL	GFDL-CM3 GFDL-ESM2G GFDL-ESM2M
NASA Goddard Institute for Space Studies	NASA GISS	GISS-E2-H GISS-E2-R
Met Office Hadley Centre (additional HadGEM2-ES realizations contributed by Instituto Nacional de Pesquisas Espaciais)	MOHC (additional realizations by INPE)	HadGEM2-ES
Institute for Numerical Mathematics	INM	INM-CM4
Institut Pierre-Simon Laplace	IPSL	IPSL-CM5A-LR IPSL-CM5B-LR
Japan Agency for Marine-Earth Science and Technology, Atmosphere and Ocean Research Institute (The University of Tokyo), and National Institute for Environmental Studies	MIROC	MIROC-ESM
Atmosphere and Ocean Research Institute (The University of Tokyo),	MIROC	MIROC5

National Institute for Environmental Studies, and Japan Agency for Marine-Earth Science and Technology		
Max-Planck-Institut für Meteorologie (Max Planck Institute for Meteorology)	MPI-M	MPI-ESM-LR MPI-ESM-MR MPI-ESM-P
Meteorological Research Institute	MRI	MRI-CGCM3
Norwegian Climate Centre	NCC	NorESM1-M

Table S1. CMIP5 model list.